NANO · MICRO small
www.small-journal.com

Nanobiosensor Reports on CDK1 Kinase Activity in Tumor Xenografts in Mice

Carmen Mihaela Tîlmaciu, Bhimareddy Dinesh, Morgan Pellerano, Sebastien Diot, Mélanie Guidetti, Julien Vollaire, Alberto Bianco, Cécilia Ménard-Moyon, Véronique Josserand,* and May C. Morris**

Probing the dynamics and quantifying the activities of intracellular protein kinases that coordinate cell growth and division and constitute biomarkers and pharmacological targets in hyperproliferative and pathological disorders remain a challenging task. Here engineering and characterization of a nanobiosensor of the mitotic kinase CDK1, through multifunctionalization of carbon nanotubes with a CDK1-specific fluorescent peptide reporter, are described. This original reporter of CDK1 activity combines the sensitivity of a fluorescent biosensor with the unique physico-chemical and biological properties of nanotubes for multifunctionalization and efficient intracellular penetration. The functional versatility of this nanobiosensor enables implementation to quantify CDK1 activity in a sensitive and dose-dependent fashion in complex biological environments in vitro, to monitor endogenous kinase in living cells and directly within tumor xenografts in mice by fluorescence imaging, thanks to a ratiometric quantification strategy accounting for response relative to concentration in space and in time.

1. Introduction

One of the challenges of modern biology and medicine is to visualize biomolecules in their natural environment, in real-time and in a noninvasive fashion, so as to gain insight into their physiological behavior and highlight alterations in clinically-relevant pathological settings. Moreover, the development of personalized medicine and targeted therapies calls for sensitive and selective means of detecting specific biomarkers in healthy versus pathological cells, so as to propose novel strategies for early-stage diagnostics, for monitoring disease progression and response to administration of therapeutics. Today, there is an urgent need for innovative sensing technologies, which allow for sensitive, rapid, and noninvasive detection of biomarkers in situ, including intracellular enzymatic activities whose deregulation is associated with disease. In particular, protein kinases constitute an important class of enzymes, hyperactivation of which contributes and sustains human cancers, thereby constituting established biomarkers and attractive pharmacological targets.[1,2] Cyclin-dependent kinases are heterodimeric serine/threonine protein kinases that play a central role in coordination of cell growth and division and participate in a wide variety of essential biological processes including transcription, tissue differentiation during development, metabolism, and neuronal function.[3,4] Altered activity of several cyclin-dependent kinases has been well documented in a large number of cancers and their contribution to stimulate and sustain unrestricted cell proliferation.[5–7] As such they constitute attractive pharmacological targets for anticancer therapeutics.[8,9] In particular, CDK1 constitutes the only essential CDK, responsible for coordination of the G2/M transition and progression through mitosis.[10,11] However, despite the oncological relevance, prognostic value and pharmacological attractivity of cyclin-dependent kinases, diagnostic approaches for detecting and quantifying alterations in their activities are poorly developed, and there is a general lack of resources to monitor these biomarkers directly in situ. Probing intracellular protein kinases in their natural environment and quantifying their relative activity remains very challenging both in terms of specificity and sensitivity. Moreover, development of noninvasive sensing technologies to assess the activity of these biomarkers remains largely limited by intracellular penetration. Until the design of fluorescent kinase activity reporters, detection of protein kinase activity was essentially limited to indirect antigenic approaches enabling detection of phosphorylated substrates of the kinase of interest, following cell or tissue fixation or extraction, such as Western blotting and immunohistochemistry. Fluorescent

Dr. C. M. Tîlmaciu, Dr. M. Pellerano, S. Diot, Dr. M. C. Morris
Institut des Biomolécules Max Mousseron-CNRS
UMR5247
Université de Montpellier
Montpellier 34093, France
E-mail: may.morris@umontpellier.fr
Dr. B. Dinesh, Dr. A. Bianco, Dr. C. Ménard-Moyon
CNRS, Immunology, Immunopathology and Therapeutic Chemistry
UPR 3572, University of Strasbourg, ISIS
Strasbourg 67000, France
E-mail: c.menard@ibmc-cnrs.unistra.fr
Dr. M. Guidetti, Dr. J. Vollaire, Dr. V. Josserand
Institut pour l'Avancée des Biosciences
INSERM U1209
CNRS UMR-5309
Université Grenoble Alpes
Grenoble 38000, France
E-mail: veronique.josserand@univ-grenoble-alpes.fr
The ORCID identification number(s) for the author(s) of this article can be found under https://doi.org/10.1002/smll.202007177.

DOI: 10.1002/smll.202007177

biosensor technologies constitute powerful and sensitive tools for direct measurement of kinase activities, thereby providing promising perspectives for early detection of target dysregulation in disease, for "smart and personalized" diagnostics.[12,13] However, while genetically-encoded fluorescence resonance energy transfer biosensors require transfection into living cells to image the dynamic behavior of protein kinases, peptide- or protein-based biosensors engineered through incorporation of environmentally-sensitive synthetic probes are more suited to quantify sensitive differences in kinase activity but remain more challenging to be introduced efficiently in living cells and organisms.[14,15]

We previously developed a fluorescent biosensor technology enabling quantification of relative CDK/Cyclin activity (CDKACT) in cell extracts. CDKACT biosensors are synthetic modular peptides comprising a phosphoamino acid binding domain (PAABD) and a substrate derived moiety onto which an environmentally-sensitive dye is conjugated. Following phosphorylation by the CDK/Cyclin kinase, fluorescence emission of the biosensor is enhanced, due to local changes in fluorophore environment, prompted by interactions between the PAABD and the phosphorylated substrate. We have shown that these tools constitute sensitive and selective tools to report on CDK/Cyclin activities in vitro, but require complementary technologies to mediate their efficient intracellular delivery for application in living cells.[16–18] In this respect, carbon nanotubes (CNTs) provide several attractive opportunities to enable application of fluorescent biosensors to image kinase activity in living cells and animal models. Due to their outstanding optical, mechanical, electrical, and thermal properties, CNTs constitute alluring materials for biological applications[19–21] such as drug delivery,[22] photothermal therapy,[23] biosensing,[24,25] and tissue engineering.[26] In particular, thanks to their high specific surface area, they constitute functionalizable platforms, scaffolds of choice for immobilization, or covalent conjugation of a wide variety of bioactive molecules including peptides, antibodies, and protein receptors.[27–30] CNTs have shown a remarkable capacity to be internalized in cells through crossing the cell membranes within minutes by direct translocation into the cytoplasm or via an energy-dependent mechanism, such as endocytosis.[31] In addition, precise control of their surface chemistry enables engineering of multimodal nanotubes and reduction of their pathogenicity.[32–34]

In this study, we report on the development of CNT-peptide biosensor conjugates designed to report and quantify relative activity of CDK1 kinase in vitro, in living cells, and in vivo. We describe conjugation of a fluorescent CDK1-specific peptide biosensor at the outer surface of multi-walled CNTs (MWCNTs), in vitro characterization and their implementation to quantify CDK1 activity in living cells and in mice bearing melanoma tumor xenografts by fluorescence imaging.

2. Results

2.1. Engineering a CNT-Peptide Biosensor That Reports on CDK1/Cyclin B1 Activity

We previously developed a toolbox of bipartite polypeptide biosensors comprising a CDK substrate sequence associated with a PAABD derived from Polo kinase, and a shorter version derived from the WW of the prolyl isomerase Pin1.[16–18] These fluorescent protein and peptide biosensors report on CDK/Cyclin activities through sensitive changes in fluorescence intensity of environmentally-sensitive dyes conjugated to the substrate moiety of the biosensor in response to kinase activities that phosphorylate the substrate. In order to develop a CDK1-specific peptide biosensor, we designed and synthesized a peptide reporter comprising a substrate sequence derived from the autophosphorylation site of Cyclin B1 by CDK1[35] and a PAABD derived from the WW domain of Pin1 (**Figure 1**A) and further designed a strategy to engineer a CDK1 nanobiosensor through multifunctionalization of MWCNTs (Figure 1B). Specifically, a first generation of CNT-peptide biosensor conjugates was prepared between MWCNTs functionalized by amidation with a COOH-terminated triethylene glycol (TEG) hydrophilic linker and the N-terminal lysine side chain amine of CDKACT1-Rhodamine peptide (CDKACT1-Rhoda) (Figure 1C; Figure S1A, Supporting Information). First, carboxylic acid groups were introduced on the nanotubes, mainly at the tips, by oxidizing MWCNTs using a (3:1) mixture of sulfuric acid and nitric acid under sonication, which yielded short nanotubes with an average length of ≈270 nm that were highly dispersible in water (Figure S1B, Supporting Information). The oxidized MWCNTs (ox-MWCNTs) were derivatized with a Boc-monoprotected TEG diamine by amidation via activation of the carboxylic acids using oxalyl chloride followed by Boc deprotection using HCl to yield *f*-MWCNTs 4. Successive derivatization of the amino groups with succinic anhydride yielded *f*-MWCNTs 5. Amine loading determined by the colorimetric Kaiser test was 203 and 58 μmol g^{-1} for *f*-MWCNTs 4 and 5, respectively. The lower amine loading confirmed the successful functionalization of the amino functions with succinic anhydride. Next, the COOH groups of *f*-MWCNTs 5 were activated using *N*-hydroxysuccinimide (NHS) allowing the reaction with the lysine side chain at the N-terminus of the CDKACT1-Rhoda biosensor peptide giving *f*-MWCNTs 6a. The CNT-peptide biosensor conjugate was characterized by thermogravimetric analysis (TGA) and transmission electron microscopy (TEM). TGA was performed under an inert atmosphere to evaluate the degree of functionalization (Figure S1C, Supporting Information). The pristine CNTs were stable up to 800 °C, while ox-MWCNTs 1 showed an increased weight loss due to the release of the carboxylic groups from the nanotube surface. The weight loss further increased after derivatization by amidation and peptide conjugation. The amount of peptide on the CNTs corresponded to the weight loss difference between *f*-MWCNTs 6a and 5 at 500 °C (9.8 μmol of peptide per gram of CNT conjugate). TEM analysis showed that the morphology of the nanotubes was not affected by the different chemical treatments (Figure S1B, Supporting Information).

2.2. Monitoring Response of CNT-CDKACT1-Rhoda Conjugate to Kinase Activity In Vitro

CNT-CDKACT1-Rhoda conjugate was first characterized in vitro to assess their response to recombinant CDKs and HeLa cell extracts as a source of CDK kinase activity.

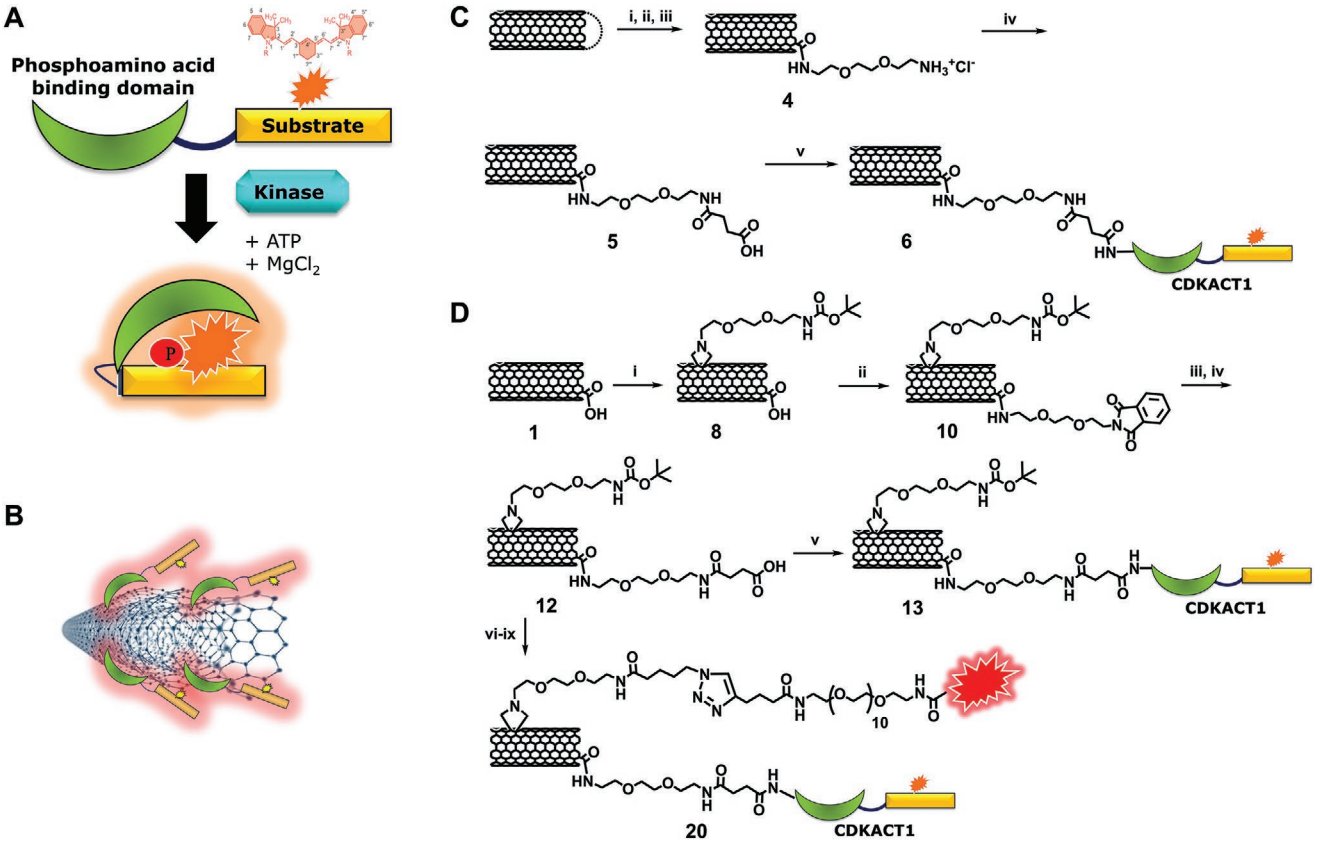

Figure 1. CDKACT1 biosensor and multifunctionalized nanobiosensor. A) Schematic representation of CDKACT1-Rhoda peptide biosensor. This bipartite design comprises a phosphoamino acid binding domain (PAABD) and a substrate derived from Cyclin B1. Rhodamine was conjugated onto the unique cysteine proximal to the phosphorylation site (at position-2). Upon phosphorylation of the substrate moiety by active CDK1 kinase, the PAABD recognizes the phosphorylated sequence. The interaction between the PAABD and the substrate changes the local environment of rhodamine, consequently promoting fluorescence enhancement. B) CDK1 nanobiosensor prepared through multifunctionalization of CDKACT1-Rhoda on MWCNTs. C) Synthesis of *f*-MWCNTs **6**: i) H_2SO_4/HNO_3 (3:1), sonication, 24 h; ii) a) oxalyl chloride, reflux, 24 h; b) Boc-monoprotected TEG diamine **2**, THF, reflux, 48 h; iii) HCl in 1,4-dioxane, 6 h; iv) *N*,*N*-diisopropylethylamine (DIEA), succinic anhydride, CH_2Cl_2, 1 day; v) a) *N*-(3-dimethylaminopropyl)-*N*′-ethylcarbodiimide hydrochloride (EDC·HCl), NHS, DMF, 24 h; b) peptide, H_2O/CH_3CN, 16 h. D) Synthesis of *f*-MWCNTs **13** and **20**: i) paraformaldehyde, compound **7**, DMF, 125 °C, 2 days; ii) EDC·HCl, DIEA, compound **9**, DMF, 24 h; iii) hydrazine, ethanol, 6 h; iv) succinic anhydride, DIEA, CH_2Cl_2, 1 day; v) a) EDC·HCl, NHS, DMF, 24 h; b) peptide, H_2O/CH_3CN, 16 h. vi) HCl in 1,4-dioxane, 6 h; vii) 5-azidopentanoic acid, EDC·HCl, hydroxybenzotriazole (HOBt), DIEA, DMF, 1 day; viii) Compound **16**, $CuSO_4{\cdot}5H_2O$, sodium ascorbate, H_2O/MeOH, 2 days; ix) a) EDC·HCl, NHS, DMF, 24 h; b) CDKACT1-Cy5 peptide, H_2O/CH_3CN, 16 h.

In order to validate the specific response of CNT-CDKACT1-Rhoda to CDK1 activity, we first compared its response to recombinant CDK1/Cyclin B1 and to the closely related CDK2/Cyclin A (**Figure 2**A,B). The optimal conditions for biosensor response were determined in two sets of dose-dependent experiments using a fixed concentration of CDK1/Cyclin B1 (75 nM) and varying concentrations of CNT-CDKACT1-Rhoda biosensor from 0 to 500 nM (corresponding to 0–51 μg mL^{-1} of CNTs), and conversely a fixed concentration of CNT-CDKACT1-Rhoda biosensor (250 nM fluorescent peptide) and different concentrations of recombinant CDK1/Cyclin B1 (Figure S2, Supporting Information). These experiments revealed that the CNT-CDKACT1-Rhoda conjugate responded to CDK1 activity in a more sensitive and robust fashion than CDKACT1-Rhoda peptide biosensor alone at the same molar concentration (determined by quantifying peptide fluorescence), with optimal response observed for 250 nM CNT-CDKACT1-Rhoda. Neither CNT-CDKACT1-Rhoda conjugate nor CDKACT1-Rhoda peptide biosensor alone responded to CDK2 activity in similar dose-dependent manner, irrespective of biosensor or kinase concentration, indicative of specific peptide biosensor response to CDK1 over CDK2, as expected from its initial design derived from the autophosphorylation sequence of Cyclin B1 (Figure S3, Supporting Information). As a negative control, the CDKACT1 peptide labelled with Dylight650 (Dy650) revealed the importance of an environmentally-sensitive probe such as rhodamine for biosensor response to kinase activity, as previously reported for CDKACT4 and CDKACT5 biosensors.[17,18]

We further evaluated the ability of CNT-CDKACT1-Rhoda to report on CDK1 activity in HeLa cell extracts as a source of kinase activity. Again, dose-dependent characterization of CNT-CDKACT1-Rhoda was performed with a fixed concentration of HeLa cell extract (40 μg) incubated with different concentrations of CNT-CDKACT1-Rhoda biosensor from 0 to 750 nM and conversely a fixed concentration of CNT-CDKACT1-Rhoda

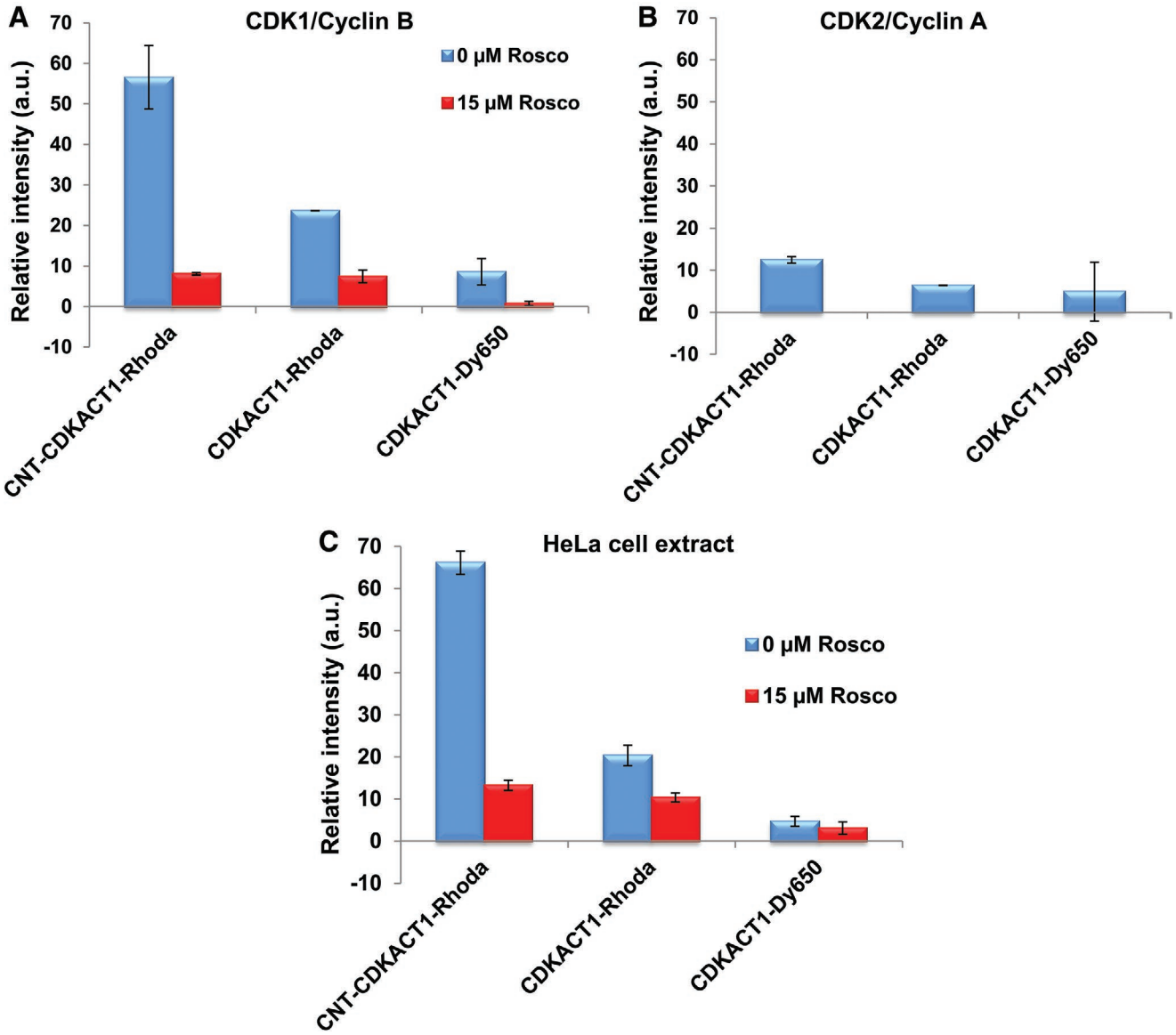

Figure 2. Response of CNT-CDKACT1-Rhoda to CDK1 and CDK2 kinase activity in vitro. A) Response of 250 nM CNT-CDKACT1-Rhoda to 75 nM recombinant CDK1/Cyclin B1 with or without 5 μM Roscovitine. B) Response of 250 nM CNT-CDKACT1-Rhoda to 100 nM recombinant CDK2/Cyclin A. C) Response of 250 nM CNT-CDKACT1-Rhoda to 40 μg HeLa cell extract with or without 5 μM Roscovitine.

biosensor and different concentrations of HeLa cell extracts from 0 to 80 μg (Figure 2C; Figure S4A, Supporting Information). As observed with recombinant CDK1/Cyclin B1, response of CNT-CDKACT1-Rhoda conjugate to CDK1 activity in HeLa cell extracts was far more significant than that of CDKACT1-Rhoda peptide biosensor at the same molar concentration (determined by quantifying peptide fluorescence) and CDKACT1-Dy650 served as a negative control to validate the importance of rhodamine in the optical transduction of kinase activity (Figure S4A, Supporting Information).

Last but not least, we verified whether the response of CNT-CDKACT1-Rhoda conjugate to recombinant CDK1/Cyclin B1 or to CDK1 in HeLa cell extracts was abolished by the pan-CDK inhibitor Roscovitine, thereby confirming that CDKACT1-Rhoda peptide biosensor and CNT-CDKACT1-Rhoda conjugate indeed responded to CDK1 activity, rather than simply detecting its presence (Figure 2A,C; Figure S4B, Supporting Information).

Taken together, these experiments revealed the superior response of CNT-CDKACT1-Rhoda conjugate over CDKACT1-Rhoda peptide biosensor alone.

2.3. Cellular Uptake and Fluorescence Imaging of CNT-CDKACT1-Rhoda Response to CDK1 Activity in HeLa Cells

Following in vitro characterization, CNT-CDKACT1-Rhoda conjugate was introduced into cultured HeLa cells for further evaluation in a cellular environment. First, the optimal conditions of CNT-CDKACT1-Rhoda internalization for imaging in

HeLa cells were determined by overlaying different concentrations of conjugates dispersed in water/glucose by sonication and varying the kinetics of cellular uptake (CNT-biosensor overlay on cells) as well as the recovery (time following overlay). Cellular penetration efficiency of the CNT-biosensor conjugate in living cells was evaluated by fluorescence microscopy. Homogeneous internalization and biosensor fluorescence was observed using submicromolar concentrations (typically 0.5 μM) of CNT-CDKACT1-Rhoda overlaid on cells for 20 min, and observed after 45 min recovery (**Figure 3**A; Figure S5A, Supporting Information). In comparison, CDKACT1 peptide alone, unconjugated to CNTs, was essentially unable to enter cells.

To further validate the ability of CNT-CDKACT1-Rhoda to report on CDK1 activity following internalization into HeLa cells we quantified its fluorescence emission prior to and following 24 h treatment with the CDK inhibitor Roscovitine (Figure 3B). Specifically, ratiometric quantification of rhodamine fluorescence relative to fluorescence of Hoechst nuclear staining in HeLa cells which had been treated with Roscovitine was significantly reduced and almost completely abolished compared to relative rhodamine/Hoechst fluorescence in untreated HeLa cells (Figure 3D). For comparison the relative fluorescence of CDKACT1-Rhoda/Hoechst following overlay on HeLa cells in the same conditions as for the CNT-biosensor conjugate was not only significantly reduced, as the peptide alone did not penetrate cells, there was essentially no difference between untreated and Roscovitine-treated cells (Figure 3C,D). These experiments revealed that the CNT-CDKACT1-Rhoda biosensor can be used to monitor alterations in CDK1 activity in living cells by fluorescence microscopy.

We further asked whether the CNT-CDKACT1-Rhoda nanobiosensor might induce any toxicity following internalization into cultured cells. To this aim, cell viability studies were performed in HeLa cells by crystal violet staining, so as to compare untreated cells and mock-treated cells, which were treated with 5% glucose/PBS, CNT-CDKACT1-Rhoda or the precursor *f*-MWCNTs 5 devoid of peptide. The concentration of CNT conjugate was 51 μg mL^{-1}, corresponding to 0.5 μM of peptide, because it is the concentration used for the observation of the fluorescence signal and the determination of the kinase activity

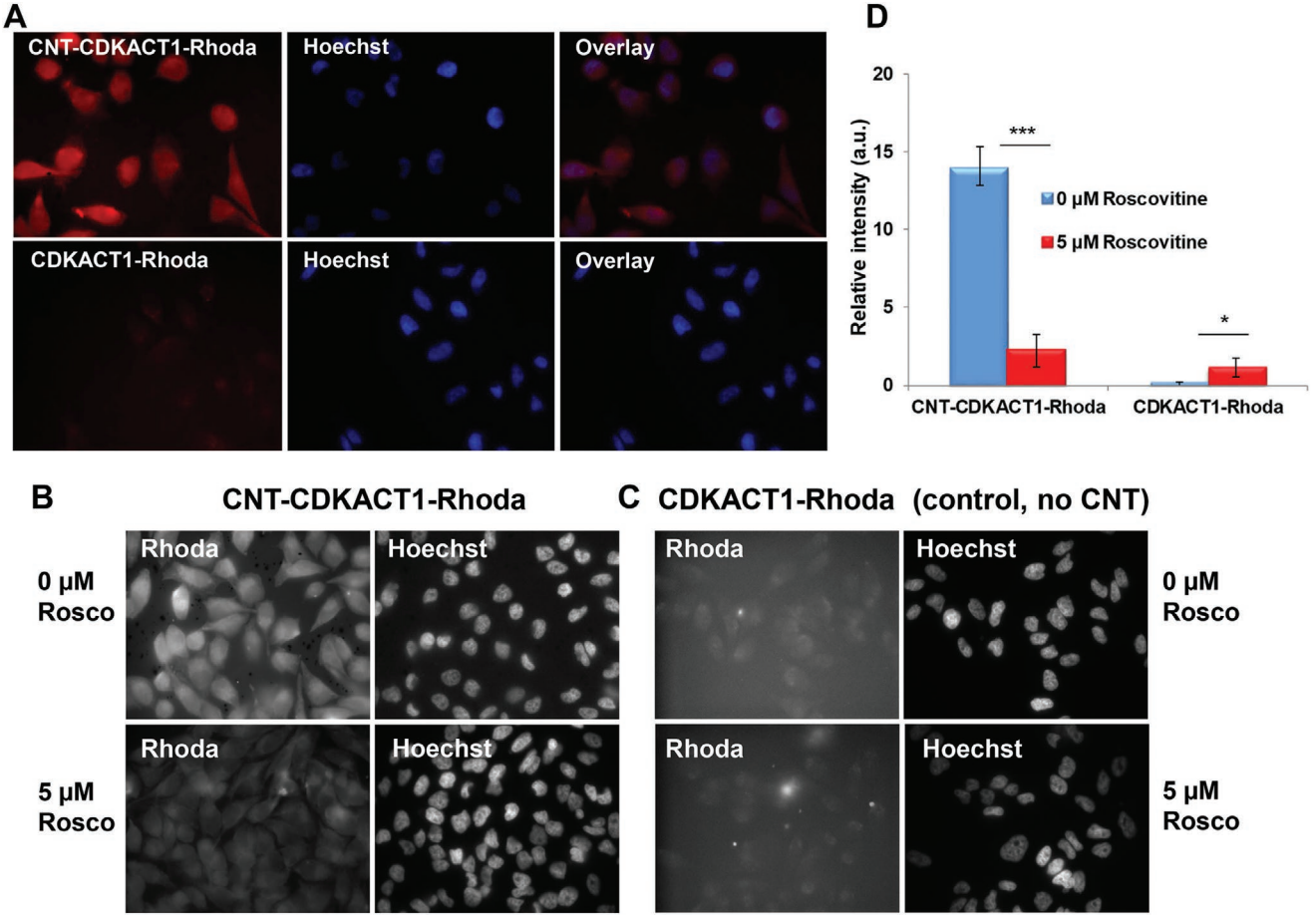

Figure 3. Cellular internalization and response to endogenous CDK kinase activity. A) 20 min overlay of 0.5 μM CNT-CDKACT1-Rhoda (corresponding to 51 μg mL^{-1} of CNTs) (upper panels) and CDKACT1-Rhoda (lower panels) on HeLa cells followed by formalin fixation, nuclear staining with Hoechst and fluorescence imaging. B) Internalization of 0.5 μM CNT-CDKACT1-Rhoda overlaid onto HeLa cells as described in (A) following mock treatment or treatment with 5 μM Roscovitine for 24 h, fixed with formalin and stained with Hoechst. C) Overlay of CDKACT1-Rhoda onto HeLa cells as described in (A), following mock treatment or treatment with 5 μM Roscovitine for 24 h, fixed with formalin and stained with Hoechst. D) Ratiometric quantification of CNT-CDKACT1-Rhoda and CDKACT-Rhoda fluorescence in (B) and (C) relative to Hoechst fluorescence.

in cultured cells. The cell viability studies revealed that cells treated with MWCNTs whether conjugated or not to CDKACT1 retained 80% viability after 24 h and about 70% after 48 h, relative to untreated cells (Figure S5B, Supporting Information).

2.4. Biodistribution and Fluorescence Imaging Studies of CNT-CDKACT1 in Mice

Due to the absorption and diffusion properties of light into tissues, noninvasive detection of fluorescence in mice requires using near-infrared (NIR) wavelengths (650–900 nm).[36]

To this aim, a CDKACT1-Cy5 peptide biosensor derivative and a CNT-CDKACT1-Cy5 conjugate were prepared as well as a control CNT conjugate functionalized with a control peptide (CNT-NanoCtrl-Cy5), derived from a previously described kinase-unrelated sequence that does not bind CDKs.[37] The CNT-NanoCtrl-Cy5 peptide conjugate 6b was prepared following the strategy used for the synthesis of the CNT-CDKACT1-Rhoda 6a (Figure 1C; Figure S1A, Supporting Information). Peptide loading assessed by TGA was 17.6 µmol per g of CNT conjugate (Figure S1C, Supporting Information).

CNT-NanoCtrl-Cy5 (200 µL at 6 µM as quantified by Cy5 fluorescence) was injected intravenously into mice to evaluate its biodistribution and pharmacokinetics (Figure S6A, Supporting Information). Mice showed no signs of suffering or discomfort until they were killed 24 h after injection.

The fluorescence emission of CNT-NanoCtrl-Cy5 was linear up to 10 µM without quenching and could be detected down to 275 nM, which was a sufficient sensitivity to enable noninvasive in vivo imaging in the mouse. This conjugate was eliminated at an early stage (starting 30 min after injection and during the first 5 h), mainly through the bladder and to a lesser extent through the hepatobiliary pathway. Twenty-four hours after injection, CNTs had been totally eliminated from the mouse body, resulting in a lack of residual signal in the *ex vivo* tissue analyses during which isolated organs were carefully examined and no abnormalities were observed (Figure S6A, Supporting Information). These results are consistent with previous studies using MWCNTs functionalized with different contrast agents.[38,39]

The ability of the nanobiosensor to reach the tumor after systemic injection was then evaluated in tumor-bearing mice. Mice were implanted subcutaneously with human melanoma cells (A375) and tumor growth was monitored by caliper measurements until the tumor volume reached 250 ± 26 mm^3 (Figure S6B, Supporting Information). As observed for CNT-NanoCtrl-Cy5 in healthy mice, no signs of suffering or discomfort were detected and the CNT-CDKACT1-Cy5 conjugate was eliminated through renal and urinary pathways and to a lesser extent through the hepatobiliary pathway, resulting in a very weak tumor contrast when using this administration route (Figure S6B, Supporting Information). Ex vivo tissue analyses 5 h after the injection evidenced no abnormalities and corroborated the in vivo observations by showing residual fluorescence mainly in the kidney, intestine, liver and only very modestly in the tumor, skin, and spleen (Figure S6B, Supporting Information).

To further concentrate the signal in the tumor, the CNT-NanoCtrl-Cy5 conjugate was injected directly into the tumor (100 µL at 1 µM as determined by quantification of Cy5 fluorescence) and noninvasive fluorescence imaging was used to monitor tumor retention of this control conjugate (**Figure 4**). The CNT-NanoCtrl-Cy5 conjugate was slowly washed out from the tumor as evidenced by 82 ± 7% fluorescence in the tumor 1 h after injection and more than 50% fluorescence still present in the tumor 2 h after injection.

In order to develop a strategy for quantitative monitoring of CDK1 activity in vivo, the relative concentration of biosensor present in the tumor at a given time had to be integrated into the quantification procedure. To this end, we first established conditions for co-injection and simultaneous detection of two conjugates in vivo in mice, the one reporting on CDK1 activity (CNT-CDKACT1-Cy5), the other simply reporting on the presence of CNT conjugates and serving as a control for normalizing the fluorescence signal of the biosensor relative to its in vivo distribution and in particular its concentration in the tumor, and this, regardless of the tumor volume. To this aim, and since fluorescence spectra of both fluorophores had to be sufficiently separated to be well discriminated for fluorescence signal quantification, a control CNT conjugate functionalized with the control peptide labelled with Dylight755 (CNT-NanoCtrl-Dy755) was prepared.

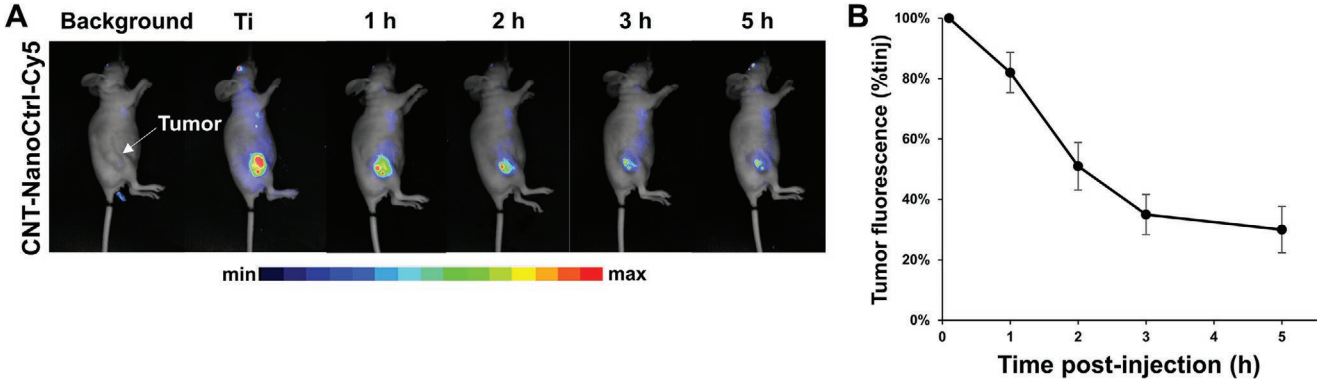

Figure 4. In vivo tumor retention of CNT-NanoCtrl-Cy5 conjugate. A) In vivo fluorescence imaging of CNT-NanoCtrl-Cy5 (excitation: 640 ± 15 nm; signal collection 680 ± 10 nm) at various time points after intratumoral injection (100 µL at 1 µM as quantified by Cy5 fluorescence, corresponding to 5.7 µg of functionalized CNTs) in subcutaneous tumor (A375)-bearing mice. B) Kinetics of tumor fluorescence signals after intratumoral injection of CNT-NanoCtrl-Cy5. Data are represented as the percentage of the signal measured 5 min after injection (T_i).

The CNT-CDKACT1-Cy5 nanobiosensor and CNT-NanoCtrl-Dy755 control were prepared by implementing a double functionalization strategy involving combination of amidation and 1,3-dipolar cycloaddition (Figure 1D; Figure S7A, Supporting Information), so as to enable a second step of CNT functionalization at a later stage with both CDKACT1-Cy5 biosensor peptide and a separate fluorophore to yield a unique double-fluorescent conjugate for self-ratiometric quantification. The ox-MWCNTs 1 were functionalized first by 1,3-dipolar cycloaddition of in situ generated azomethine ylides and then by amidation between the carboxylic acids at the tips and a phthalimide-monoprotected TEG diamine linker. The Pht group on *f*-MWCNTs 10 was deprotected by treating with hydrazine and the amine loading assessed by the Kaiser test was 87 μmol g^{-1}. Successive reaction with succinic anhydride led to a reduced Kaiser test value (20 μmol g^{-1}) confirming the successful amine derivatization. The CNT-CDKACT1-Cy5 13a and CNT-NanoCtrl-Dy755 13b were prepared by conjugating the corresponding dye-labelled peptides to *f*-MWCNTs 12 after NHS activation. The level of functionalization was 28.9 and 16.9 μmol g^{-1} for *f*-MWCNT 13a and 13b, respectively, based on TGA (Figure S7B, Supporting Information).

Like the rhodamine-labelled biosensor peptide, the Cy5-labelled CNT-CDKACT1 derivative responded to CDK1 kinase activity in vitro using HeLa cell extracts as a source of kinase (Figure S8A, Supporting Information) and both CNT-CDKACT1-Cy5 and CNT-NanoCtrl-Dy755 were efficiently internalized in living HeLa cells (Figure S8B, Supporting Information).

Subsequently, seven mice with subcutaneous A375 melanoma tumors received an intratumoral co-injection of CNT-CDKACT1-Cy5 and CNT-NanoCtrl-Dy755 conjugates (25 μL at 10 μM each as quantified by the absorbance of their fluorescent probe) and dual fluorescence imaging at suitable wavelengths was performed immediately after injection (T_i), then 1 and 2 h post-injection (**Figure 5**A). At each imaging time point CNT-nanobiosensor/CNT-control conjugate fluorescence ratio was calculated (CNT-CDKACT1-Cy5/CNT-NanoCtrl-Dy755) and expressed as a percentage of the T_i ratio obtained immediately after the injection. Thus, any increase in this ratio reports on nanobiosensor response to CDK1 kinase activity relative to the concentration of CNT conjugates, that is, independently of its biodistribution. The two conjugates showed clearly distinct fluorescence signal kinetics, CNT-NanoCtrl-Dy755 showing a fluorescence decay in relation to its elimination from the tumor (as previously observed for CNT-NanoCtrl-Cy5) and CNT-CDKACT1-Cy5 exhibiting an increase in fluorescence related to biosensor response to CDK1 activity. Ratiometric quantification/analysis of these two fluorescence kinetics results in a Cy5/Dy755 ratio increase by a factor of 3.5 during the first hour post-injection thereby clearly validating nanobiosensor response to CDK1 activity within the tumor tissue (Figure 5B).

To enable ratiometric quantification of nanobiosensor response to CDK1 activity relative to its concentration in space and time using one single conjugate comprising two distinct fluorescent species (biosensor and probe for signal normalization), we finally prepared double-fluorescently-labelled CNT conjugate by functionalizing CNTs with both CDKACT1-Cy5 peptide and Alexa Fluor 750 (Alexa750) as control probe. We unfortunately first experienced fluorescence quenching when Alexa750 dye was coupled directly to CNTs through the TEG linker probably due to energy/charge transfer between the dyes because of their close proximity. Hence, we designed an alternative strategy to conjugate the fluorophore by using click chemistry. To this aim, a modified PEG_{10} linker bearing an alkyne moiety at one end and Alexa750 at the other end was synthesized (Figure S9A, Supporting Information). After Boc cleavage of the double functionalized MWCNTs 12 in acidic conditions, the amino groups were derivatized by amidation with 5-azidopentanoic acid (Figure 1D; Figure S9B, Supporting Information). The copper-catalyzed azide-alkyne cycloaddition

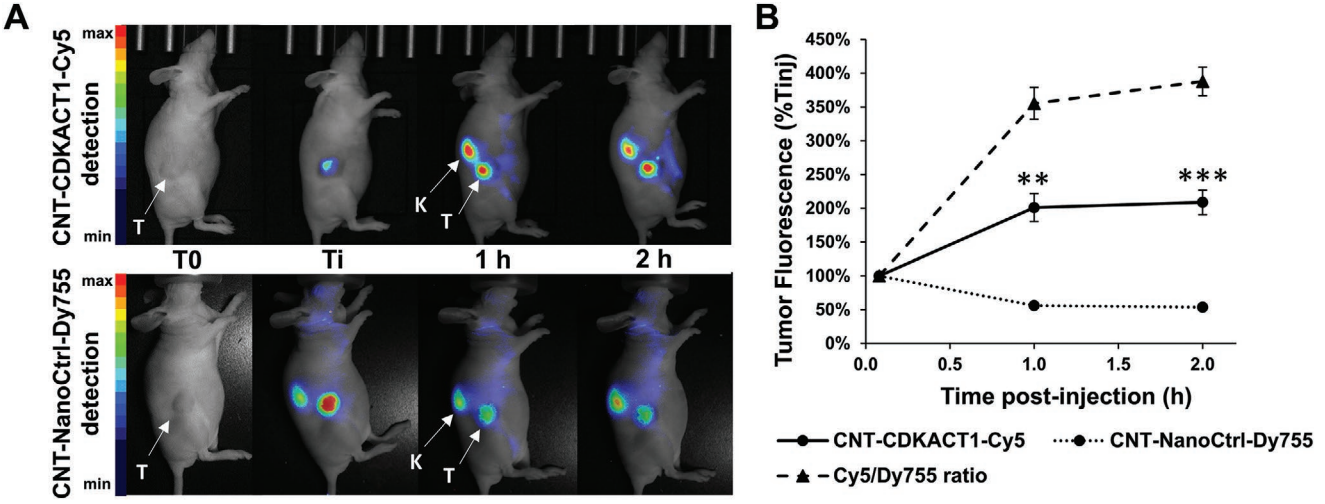

Figure 5. Noninvasive imaging of CDK biosensor fluorescence in tumor-bearing mice. A) In vivo dual fluorescence imaging of CNT-CDKACT1-Cy5 (excitation: 640 ± 15 nm; signal collection: 680 ± 10 nm) and CNT-NanoCtrl-Dy755 (excitation: 780 nm; signal collection: >830 nm) immediately (T_i), 1 and 2 h after their co-injection in the tumor (25 μL at 10 μM each as quantified by the fluorescent probe, corresponding to 8.7 and 14.8 μg CNT-CDKACT1-Cy5 and CNT-NanoCtrl-Dy755, respectively). K = kidney and T = tumor. B) Kinetics of Cy5 and Dy755 fluorescence signals in the tumor after co-injection of CNT-CDKACT1-Cy5 (solid line) and CNT-NanoCtrl-Dy755 (dotted line) $n = 7$ mice. Statistical analyses: Bonferroni's multiple comparisons test (**p-value < 0.01; ***p-value < 0.001). In vivo CDKACT1 biosensor response is reported by Cy5/Dy755 fluorescence ratio in the tumor (dashed line).

(CuAAC) reaction was performed between azido-MWCNTs 18 and the alkyne-PEG-Alexa750 linker 16 using a catalytic amount of copper(II) sulfate and sodium ascorbate to yield Alexa750-labelled *f*-MWCNTs 19. The activation of the COOH groups with NHS followed by amidation with CDKACT1-Cy5 peptide yielded nanobiosensor 20 with a level of functionalization of 18.0 µmol g^{-1} according to TGA (Figure S9C, Supporting Information).

The double-labelled nanobiosensor 20 was injected into melanoma tumors and dual fluorescence imaging at suitable wavelengths was performed immediately after injection (T_i), then 30 min, 1 h, and 2 h post-injection (**Figure 6**A). Mice injected with the nanobiosensor showed an increase in Cy5 fluorescence emission associated with only a very weak variation in the Alexa750 signal (Figure 6B), resulting in a net increase in the Cy5/Alexa750 fluorescence ratio indicative of biosensor response to CDK1 activity within tumor xenografts (Figure 6C).

To confirm whether the nanobiosensor could further report on physiological variations of CDK1 activity directly in vivo, eight mice were treated twice by intraperitoneal co-injection of the pan-CDK inhibitor Roscovitine (50 mg kg^{-1}) and the CDK1-inhibitor RO-3306 (4 mg kg^{-1}) first for one day and then again for 1 h, before injection of nanobiosensor 20, while eight other mice received the vehicle only. Roscovitine is a pan-CDK

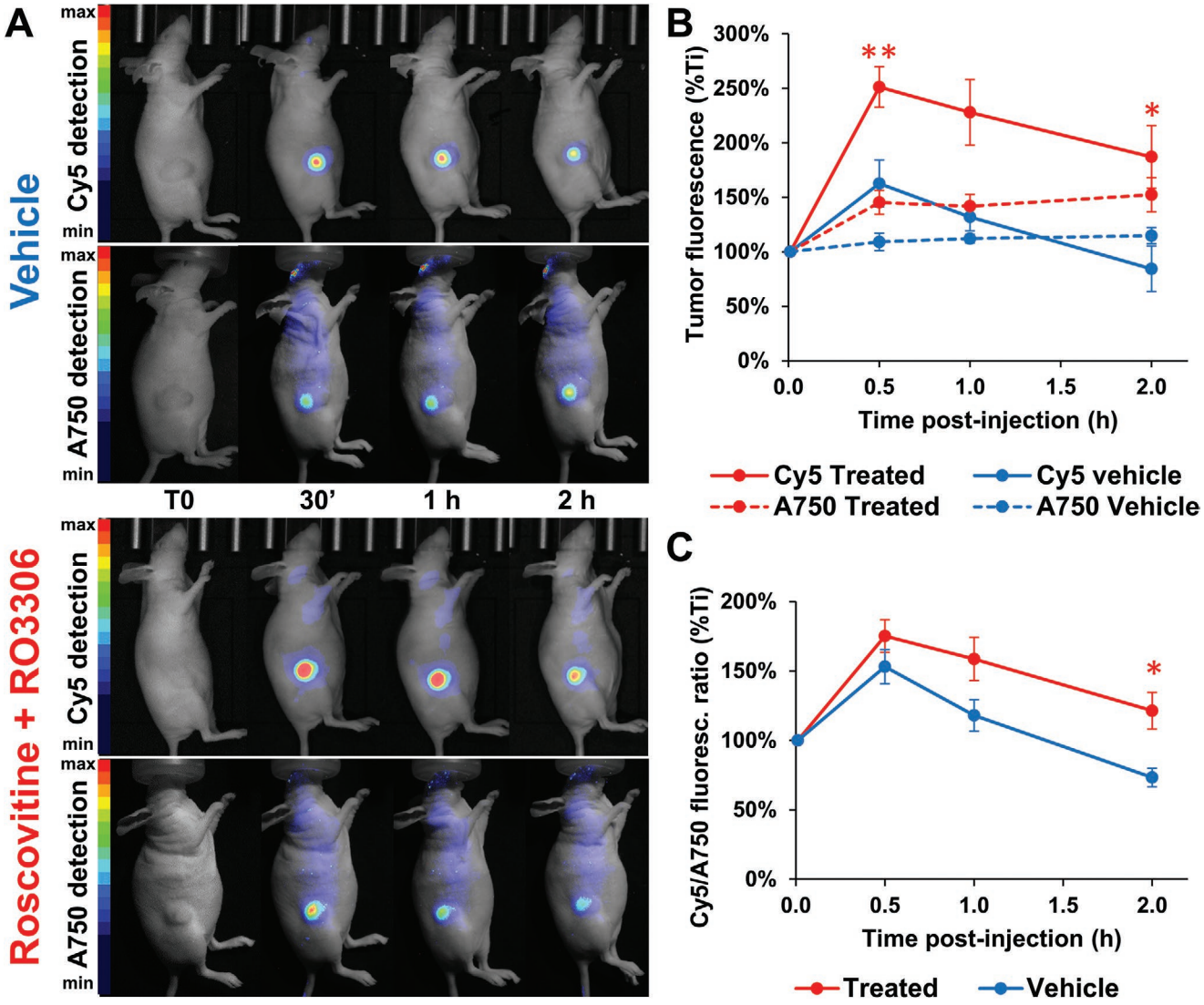

Figure 6. Modulation of CDK activity in vivo in tumor-bearing mice evidenced by noninvasive fluorescence imaging. In vivo dual fluorescence imaging of tumor-bearing mice (subcutaneous A375 melanoma) treated by intraperitoneal injection of Roscovine (50 mg kg^{-1}) and RO-3306 (4 mg kg^{-1}) twice, first for one day and then again for 1 h before injection of nanobiosensor 20 in the tumor (50 µL at 9 µM as quantified by the absorbance of their fluorescent probe, corresponding to 25 µg CNT conjugate). A) Dual fluorescence imaging was performed using 640 ± 15 nm excitation and 680 ± 10 nm emission for Cy5 detection, and 680 nm excitation and >700 nm emission for Alexa750 detection, immediately (T_i), 30 min, 1 h, and 2 h after nanobiosensor 20 injection. B) Kinetics of Cy5 (solid lines) and Alexa750 (dotted lines) fluorescence emission in the tumor after nanobiosensor 20 injection in treated (red lines) or nontreated (blue lines) mice. $n = 8$ mice per group. Statistical analyses: Bonferroni's multiple comparisons test (*p-value < 0.05; **p-value < 0.01). C) In vivo nanobiosensor 20 response in treated (red line) or nontreated (blue line) mice determined by Cy5/Alexa750 fluorescence ratio. $n = 8$ mice per group. Statistical analyses: Bonferroni's multiple comparisons test (*p-value < 0.05).

inhibitor, which primarily inhibits CDK2 and leads to accumulation of cells in S-phase, whereas the CDK1 inhibitor RO-3306 blocks cells at the G2/M transition.[40] The double treatment with Roscovitine and RO-3306 was initially intended to completely block CDK activity in the tumor, since previous studies had revealed intraperitoneal administration of Roscovitine alone in this melanoma tumor model was insufficient to block CDK activity completely. However, mice treated with Roscovitine and RO-3306 exhibited a significantly higher increase in the nanobiosensor Cy5 fluorescence emission compared to vehicle-treated mice (×2.5 for the treated group vs ×1.6 for the vehicle group at 30 min post-injection; $^{**}p$-value < 0.01), associated with a very slight variation in Alexa750 fluorescence (Figure 6B), resulting in an overall greater increase in Cy5/Alexa750 fluorescence ratio for the treated group compared to the vehicle group (Figure 6C). The nanobiosensor was therefore indeed capable of reporting on greater CDK1 activity in mice treated with Roscovitine and RO-3306 in these experimental conditions. This difference was most significant 2 h post-injection ($^{*}p$-value < 0.05), inferring that a minimal lapse of time was probably required for the nanobiosensor to penetrate the tumor cells and respond effectively to active CDK1 kinase. To understand why the double Roscovitine/RO-3306 treatment led to an unexpected increase in CDK1 activity, we asked whether it might be due to synchronized release of cells from a Roscovitine-induced S-phase block, resulting in simultaneous activation of CDK1/Cyclin B1, RO-3306 being insufficient to inhibit CDK1 activity when co-administrated with Roscovitine, which preferentially leads to an S-phase block. To this aim we treated cultured A375 cells with Roscovitine and RO-3306 using the same conditions as for tumor treatment in mice and examined the levels of cyclin B1 and phospho-cyclin B1, the latter being indicative of CDK1 activity and cyclin B1 autophosphorylation. Indeed, consistent with the nanobiosensor response observed in vivo, Western blot analysis of A375 cells treated for 24 h with Roscovitine or with Roscovitine and RO-3306, revealed the presence of phosphorylated Cyclin B1, associated with CDK1 activity, in contrast to a 48 h Roscovitine treatment, which completely abolished Cyclin B1 autophosphorylation. Moreover, release from a 24 h Roscovitine or Roscovitine + RO-3306 block (mimicking a likely release of tumor cells following the first treatment in vivo) followed by a second 1 h Roscovitine or Roscovitine/RO-3306 treatment, (as performed in vivo) was insufficient to inhibit CDK1 and led to further accumulation of phosphorylated Cyclin B (Figure S10, Supporting Information). These in vitro studies hence confirmed that the nanobiosensor indeed reports on CDK1 activation following release from a Roscovitine or Roscovitine/RO-3306 block, in agreement with in vivo experiments.

3. Conclusion

Together with the development of molecular imaging technologies, fluorescent biosensors constitute powerful and sensitive tools to monitor the activity of intracellular targets. Bioprobes or biosensors that can detect and report on molecular anomalies in malignant cells are of major interest for development of diagnostics and associated therapeutic strategies. In this respect, environmentally-sensitive peptide biosensors constitute attractive tools, but their application to monitor dynamic and enzymatic processes in living cells is hampered by their inability to cross cell membranes, calling for strategies to enable their intracellular delivery.

CNTs constitute efficient carriers, given their remarkable cell-penetrating capacity and constitute attractive platforms for multifunctionalization, due to their high specific surface area. In this study, we have exploited these exceptional properties to engineer an original nanobiosensor of CDK1 activity through conjugation of multiple copies of an environmentally-sensitive fluorescent peptide biosensor derived from the autophosphorylation site of Cyclin B1 at the surface of carbon nanotubes.

Not only is CNT-CDKACT1 the first CNT reporter of kinase activity, we have shown it could be implemented for fluorescence-based detection and quantification of CDK1 activity in vitro, in living cells and in vivo. Indeed, this nanobiosensor responds to active recombinant CDK1/Cyclin B1 and to endogenous kinase activity in HeLa cell extracts in a sensitive and dose-dependent fashion, penetrates efficiently into living cells and can report on kinase activity by fluorescence imaging. Furthermore, its optimization to generate a double-labelled nanobiosensor enabled us to monitor CDK1 activity in vivo within tumor xenografts, thanks to a ratiometric quantification strategy accounting for the relative concentration of the nanobiosensor in space and in time.

The originality of this nanobiosensor is that beyond simple detection of CDK1, it can report on its enzymatic activity, thereby providing information concerning kinase function in a complex environment. Since alterations in CDK/cyclin activity have been reported in a wide variety of cancers and associated with negative prognosis, we anticipate that our technology should provide a direct means of probing hyperactivation of these kinases, and of guiding therapeutic intervention/decision, thereby contributing to cancer diagnostics, assisting therapeutic programs, and monitoring response to therapeutics.

4. Experimental Section

Chemicals, Characterization Methods, and Instrumentation: Pristine multi-walled carbon nanotubes (MWCNTs) (20–30 nm diameter, 0.5–2 µm length, 95% purity; batch 1240XH) were purchased from Nanostructured and Amorphous Materials. The linker *O*-(2-aminoethyl)-*O′*-[2-(Boc-amino) ethyl]decaethylene glycol was purchased from Polypure AS company and used as it was received. Alexa Fluor 750 free acid tris(triethylammonium) salt was purchased from Fisher Scientific. The dry solvents and 4 M HCl in 1,4-dioxane were purchased from Sigma-Aldrich and were used as supplied. All other reagents were obtained from commercial suppliers and used without further purification. The CNT suspensions were sonicated in a water bath using either a Transsonics Digitals Elma sonicator (20 W, 40 kHz) or an Elmasonic P30H (37 kHz) sonicator. The Spectra/Por dialysis membrane (standard RC tubing MWCO: 12–14 kDa) was purchased from SpectrumLabs.

Functionalization of MWCNTs: The protocols for the synthesis of the precursor CNTs and the alkyne-PEG-Alexa750 linker 16 are described in the section Materials and Methods, Supporting Information.

Preparation of Functionalized MWCNTs 6a and 6b: a) NHS activation: To a suspension of *f*-MWCNTs 5 (10 mg) in anhydrous DMF (6 mL) sonicated in a water bath for 10 min, were added EDC·HCl and NHS (50 mg). The mixture was sonicated for 10 min and stirred under argon for 24 h. The reaction mixture was filtered over a PTFE membrane (0.1 µm). The solid recovered on the filter was dispersed in DMF (75 mL). The suspension was sonicated for 5 min in a water bath and

filtered. This sequence was repeated successively with DMF, methanol, and dichloromethane. The solid was dried under vacuum to give NHS-derived MWCNTs.

b) Peptide conjugation: The dye-labelled peptide NanoCtrl-Cy5 (2 mg) was solubilized in a mixture of MilliQ water (1.9 mL) and CH_3CN (0.1 mL), and the solution was then added to the NHS-derived MWCNTs (6 mg) pre-dispersed in 2 mL of MilliQ water by sonication in a water bath for 5 min. The reaction mixture was sonicated for 1 min and stirred for 16 h in the dark. The progress of the conjugation reaction was monitored by HPLC. Aliquots of 40 µL of the reaction mixture diluted with 100 µL of MilliQ water was centrifuged to analyze the supernatant solution by HPLC. The detected peak in HPLC corresponded to the unreacted peptide in the supernatant solution. After 16 h, the reaction mixture was diluted by adding 20 mL of MilliQ water and filtered over a PTFE membrane (0.1 µm). The solid recovered on the filter was dispersed again in MilliQ water and filtered. This washing sequence was repeated until the filtrate was colorless indicating that the free peptide was eliminated. Finally, the solid was dispersed in MilliQ water, the suspension was dialyzed against MilliQ water to remove any trace of free peptide and lyophilized to obtain conjugate CNT-NanoCtrl-Cy5 6b.

This protocol was followed for the preparation of CNT-CDKACT1-Rhoda conjugate 6a using the dye-labelled peptide CDKACT1-Rhoda and freshly prepared NHS-derived MWCNTs.

TEM images showed the intact morphology of the nanotubes after the different chemical treatments (Figure S1B, Supporting Information). According to TGA the peptide loading was found to be 9.8 and 17.6 µmol g^{-1} for *f*-MWCNTs 6a and 6b, respectively (Figure S1C, Supporting Information).

Preparation of functionalized MWCNTs 13a and 13b: a) NHS activation: The protocol used for NHS activation of *f*-MWCNTs 5 was applied starting from *f*-MWCNTs 12.

b) Peptide conjugation: The protocol used to synthesize *f*-MWCNTs 6a and 6b was applied for the preparation of *f*-MWCNTs 13a and 13b using 5 mg of the NHS-derived *f*-MWCNTs and 1.78 mg of dye-labelled peptide CDKACT1-Cy5 and 1.03 mg of dye-labelled peptide NanoCtrl-Dy755, respectively.

According to TGA the peptide loading was found to be 28.9 and 16.9 µmol g^{-1} for *f*-MWCNTs 13a and 13b, respectively (Figure S7B, Supporting Information). TEM analysis showed the preserved morphology of the nanotubes after the different chemical treatments (Figure S1B, Supporting Information).

Synthesis of functionalized MWCNTs 20: a) NHS activation: The protocol used for the NHS activation of *f*-MWCNTs 5 was applied starting from *f*-MWCNTs 19.

b) Peptide conjugation: A suspension of the NHS-derived MWCNTs (6 mg) in MilliQ water (2 mL) previously sonicated in a water bath for 30 s, was added to a solution of dye-labelled peptide CDKACT1-Cy5 (3.4 mg) in a mixture of MilliQ water (1.8 mL) and acetonitrile (0.2 mL). The reaction mixture was sonicated for 30 s and stirred in the dark at room temperature. The monitoring of the reaction by HPLC and the work-up were done as mentioned in the protocol for the preparation of *f*-MWCNTs 6b, giving *f*-MWCNTs 20. The peptide loading assessed by TGA was 18 µmol g^{-1} (Figure S9C, Supporting Information). TEM indicated that the different chemical treatments did not affect the morphology of the nanotubes (Figure S1B, Supporting Information).

Peptide Biosensor Design, Synthesis and Labelling: CDKACT1 and NanoCtrl peptides were synthesized by GLS Biochem and purified to 95%. They were labelled with a tenfold molar excess of rhodamine- or Cy5-maleimide, then further purified on NAP5 columns (GE Healthcare) in 50 mM TrisHCl, pH 7.4, 150 mM NaCl, to remove excess label as described previously in references.[16,17]

The sequence of CDKACT1 is: *N*-acetyl-KGWEGRMSRSSGRVYYFNHITN ASQWERPSGGGPEPILVDCSSPSPMET. The sequence of NanoCtrl peptide is *N*-acetyl-KVESSDTIDNVKSKIQDKEGC.

Dispersion of CNT-Peptide Biosensor Conjugates for Biological Experiments: CNT-peptide biosensors were dispersed in 5% glucose/H_2O at 100 µg per 100 µL stock concentrations and then diluted to the appropriate concentration required by serial dilution and sonication in a water bath for 5 min after each dilution.

SDS-PAGE and Western Blotting: SDS-PAGE was performed according to standard protocols. Proteins were transferred onto PVDF membranes (Immobilon-P, Merck Millipore) for 2 h at 100 V in precooled Towbin buffer using a liquid BioRad system. Western blotting was performed according to standard procedures: membranes were first saturated with 5% BSA in 50 mM Tris, pH 7.2, 150 mM NaCl, 0.1% Tween, then incubated overnight at 4 °C with the anti-cyclin B1 (Cell Signaling #12231), beta-actin (Cell Signaling #4967S) antibody, or the mouse anti-phospho-H3 antibody (Cell Signaling #9706) diluted 1:1000 in 50 mM Tris, pH 7.2, 150 mM NaCl, 0.1% Tween, then washed twice for 15 min with 50 mM Tris, pH 7.2, 150 mM NaCl, 0.1% Tween, and incubated for 1 h at room temperature with horseradish peroxidase-conjugated secondary antibodies (GE Healthcare) diluted 1:10 000 in 50 mM Tris, pH 7.2, 150 mM NaCl, 0.1% Tween. After three final 5 min washes with 50 mM Tris, pH 7.2, 150 mM NaCl, 0.1% Tween, membranes were processed with ECL Prime (GE Healthcare; #RPN2232) for signal detection. Protein levels were determined by quantifying pixel intensity for each band of interest relative to pixel intensity of the actin band in the same sample.

Cell Culture and Extract Preparation: Cell culture media, serum, and antibiotics were purchased from Invitrogen. HeLa and A375 cells were cultured in DMEM + Glutamax supplemented with 10% FCS, 100 units per mL penicillin (G sodium salt) and 100 µg per mL streptomycin at 37 °C in an atmosphere containing 5% CO_2. Cell extracts were prepared in PBS lysis buffer pH 7.4, 150 mM NaCl, 0.2% NP40, 1 mM EDTA, 2 mM PMSF, Complete protease inhibitors (Roche), and normalized following spectrophotometric dosage at 280 nm.

CDK1/Cyclin B1 and CDK2/Cyclin A Protein Expression and Purification: Recombinant active GST-CDK1/Cyclin B1 and GST-CDK2/Cyclin A complexes were prepared as described previously in references.[16,17] Recombinant GST-CDK1, GST-CIV, GST-CDK2/CIV, MBP-Cyclin B, and 6His-Cyclin A were expressed in *Escherichia coli* (BL21 DEA3) following induction with 1 mM isopropyl β-D-1-thiogalactopyranoside (IPTG) overnight at 20 °C. GST-CDK1, GST-CIV, and GST-CDK2/CIV were purified by FPLC on a GSTrap HP 5 mL column (GE Healthcare) equilibrated in PBS buffer (50 mM phosphate, pH 7.4, 150 mM NaCl). GST-tagged proteins were eluted with PBS buffer containing glutathione (50 mM; Euromedex), and then further injected onto a desalting column (GE Healthcare) equilibrated in their purification buffer to eliminate free glutathione. MBP-Cyclin B was purified by FPLC on an MBPTrap HP 5 mL column (GE Healthcare) equilibrated in PBS buffer (50 mM phosphate, pH 7.4, 150 mM NaCl). MBP-Cyclin B was eluted with PBS buffer containing 20 mM maltose, and then further injected onto a HiLoad 16/600 Superdex 75 prep-grade column (GE Healthcare) equilibrated in PBS buffer. Active GST-CDK1/MBP-Cyclin B complex was formed following individual purification of each subunit and stoichiometric incubation together with GST-CIV. Active GST-CDK2/6His-Cyclin A complex was formed by incubating 6His-Cyclin A with GST-CDK2/CIV on the GST affinity column, prior to elution.

In Vitro Kinase Activity Assays: Kinase assays were performed by incubating CNT-biosensor conjugates, peptide biosensor, or control CNTs with either catalytically active recombinant CDK1/Cyclin B1, CDK2/Cyclin A, or HeLa cell extracts as a source of active kinase, in the presence or absence of CDK inhibitor Roscovitine (Euromedex). Fluorescence kinase assays were performed as described previously in refs. [16,17] in 96-well plates in a chamber thermostated at 30 °C using a Clariostar spectrofluorimeter (BMG). The fluorescence of rhodamine-labelled peptide biosensor or CNT-biosensor conjugate was monitored over time in 200 µL PBS (Sigma) supplemented with 5 mM $MgCl_2$, 0.5 mM ATP at 605 nm following excitation at 550 nm. In all experiments, relative fluorescence was calculated following substraction of biosensor fluorescence (peptide alone or CNT-peptide conjugate) from fluorescence values obtained upon incubation with kinase. Data analysis was performed using the GraFit 7 Software (Erathicus Ltd). Experiments were performed in triplicate, and error bars indicate standard deviation from average.

Cell Internalization Studies, Fluorescence Imaging, and Quantification: Fluorescently labelled-biosensor peptide or CNT-biosensor conjugates were overlaid on living cells grown to subconfluency on glass coverslips for 20 min at the indicated concentrations in H_2O/glucose, and cells were then replaced in cell culture medium supplemented with serum for recovery for 30–45 min. Cells were extensively washed with PBS, stained with Hoechst, fixed with formalin, and mounted in Mowiol. Cells were imaged with a Zeiss Axioimager Z2 microscope equipped with a CoolSnap HQ2 camera and piloted by MetaMorph software. Image J was then used for image analysis and quantification of signals. Regions of interest (ROI) corresponding to 10–15 cells in which fluorescence appeared homogeneous were designed and the mean grey levels of fluorescence for each channel (Hoechst and rhodamine) were quantified within these ROIs. For each experiment, and the mean ratiometric value of rhodamine/Hoechst was calculated from 3–4 different ROIs.

Cell Viability Studies: Cell viability was evaluated by crystal violet staining at 0, 24, and 48 h as follows: cells were washed with PBS, fixed with 3.7% formaldehyde for 10 min, and then incubated with 0.1% crystal violet dye for 30 min. After rinsing, crystals were dissolved in 10% acetic acid and viability was determined by measuring absorbance at 595 nm.

In Vivo Fluorescence Imaging and Cancer Mouse Models: Animal experimentations were performed in accordance with the institutional guidelines of the European Community (EU Directive 2010/63/EU) for the use of experimental animals and received the approval of the local ethics committee (Cometh38 Grenoble, France) and the French Ministry of Higher Education and Research under the reference: apafis#8854-2017031314338357 v1.

Cancer Mouse Model: CNT-peptide conjugates were injected into mice bearing subcutaneous xenografts established from A375 melanoma cell line which express hyperactive forms of cyclin-dependent kinases. Five-week-old female NMRI nude mice (Janvier Labs, Le Genest-Saint Isle, France) were anesthetized (4% isoflurane/air for anesthesia induction and 1.5% thereafter) and were injected subcutaneously in the flank with 3×10^6 exponentially dividing A375 cells (200 µL in 1× PBS). Tumor size was measured twice a week using a caliper.

CNT-Peptide Preparation for In Vivo Administration: CNT-peptide conjugates were dispersed in water/glucose 5% to reach a CNT concentration of 1 g L^{-1} before the solution was submitted to two sonication steps of 10 and 5 min interspersed with 1 min of vortex agitation. It was then diluted in water/glucose 5% to reach the desired concentrations.

In Vivo Fluorescence Imaging in Mice: In vivo fluorescence imaging was performed using IVIS Kinetic (PerkinElmer, USA) with 640 ± 15 nm excitation and 680 ± 10 nm emission filter, Fluobeam700 (Fluoptics, France) with 680 nm excitation and >700 nm long pass filter, and Fluobeam800 (Fluoptics, France) with 780 nm excitation and >830 nm long pass filter for the detection of Cy5, Alexa750, and Dy755, respectively.

In vivo biodistribution, pharmacokinetics and elimination pathways of CNT conjugates were characterized by fluorescence imaging in mice. Six weeks old NMRI female nude mice (Janvier labs, France) were anesthetized (air/isoflurane 4% for induction and 1.5% thereafter) and whole-body fluorescence imaging was performed before, and at several time points after CNT-peptide conjugate administration. Mice were sacrificed at the final time point and organs were harvested for *ex vivo* fluorescence imaging. Organs from control mice were also exposed to the camera to set the autofluorescence level for each organ. For in vivo image analyses, ROIs were defined on the tumor and contralateral site (skin) as well as on the liver and kidney areas. For ex vivo image analyses, ROIs were adjusted on each tissue sample. Results were expressed as average fluorescence in the ROIs (average radiant efficiency [p/s/cm²/sr]/[µW/cm²]) and graphs represent the mean ± SEM for six mice.

Noninvasive Fluorescence Imaging of CDK Biosensor Activation in Tumor-Bearing Mice: Eighteen days after A375 melanoma tumor implantation, CNT-CDKACT1-Cy5 and CNT-NanoCtrl-Dy755 conjugates were co-injected into the tumor (25 µL at 10 µM each) and dual fluorescence imaging at suitable wavelengths was performed immediately after injection (T_i), then 1 and 2 h post-injection. Biosensor fluorescence was imaged and quantified with respect to control peptide fluorescence. At each imaging time point, CNT-biosensor/CNT-control conjugate fluorescence ratio was calculated (CNT-CDKACT1-Cy5/CNT-NanoCtrl-Dy755) and expressed as a percentage of the T_i ratio obtained immediately after the injection.

Modulation of CDK Activity In Vivo in Tumor-Bearing Mice Evidenced by Noninvasive Fluorescence Imaging: When A375 melanoma subcutaneous tumors reached a volume of about 250 mm^3, mice were treated by intraperitoneal injection of Roscovitine (50 mg kg^{-1}) and RO-3306 (4 mg kg^{-1}) or vehicle (30% DMSO; 25% Diluent (Tween 80, *N-N*-dimethylacetamide, PEG 400 (proportion: 1-2-7) and 45% PBS)) one day and 1 h before injection of nanosensor 20 in the tumor (50 µL at 9 µM). Dual fluorescence imaging at suitable wavelengths was performed immediately after injection (T_i), then 30 min, 1 h, and 2 h post-injection. At each imaging time point, Cy5/Alexa750 fluorescence ratio was calculated and expressed as a percentage of the T_i ratio obtained immediately after the injection.

Supporting Information

Supporting Information is available from the Wiley Online Library or from the author.

Acknowledgements

The authors thank Alexane Caignard for help with the preparation of one CNT conjugate. The authors thank C. Royer and V. Demais for help with TEM analyses at the "Plateforme Imagerie in vitro" at the Center of Neurochemistry (INCI, Strasbourg, France). The authors thank Jean-Luc Coll for critical reading of the manuscript. This work was supported by the CNRS (Centre National de la Recherche Scientifique) and a grant from the French National Research Agency (ANR) (NANOMULTISENS Project Grant No. ANR-13-BS10-0003). C.-M.T. and B.D. were funded by the ANR. The authors acknowledge the MRI imaging facility (Montpellier, France), a member of the national infrastructure France-BioImaging supported by the French National Research Agency (ANR-10-INBS-04, Investissements d'avenir). The Optimal imaging platform is supported by France Life Imaging (French program "Investissement d'Avenir" grant; "Infrastructure d'avenir en Biologie Santé", ANR-11-INBS-0006) and the IBISA French consortium "Infrastructures en Biologie Santé et Agronomie." This work was partly supported by the ANR through the LabEx project Chemistry of Complex Systems (ANR-10-LABX-0026_CSC), and by the International Center for Frontier Research in Chemistry (icFRC).

Conflict of Interest

The authors declare no conflict of interest.

Author Contributions

C.-M.T. and B.D. contributed equally to this work. B.D. performed experiments involving conjugation and purification of CNT-peptide biosensors. C.-M.T., M.P., and S.D. performed peptide biosensor labelling, purification and characterization, recombinant protein kinase expression and purification, in vitro kinase assays, cell culture and cell extract preparation, fluorescence microscopy studies of nanobiosensor internalization, and quantification in living cells. M.G., J.V., and V.J. prepared animals, xenografts, and performed animal imaging studies. M.C.M, C.M-M., A.B., and V.J. supervised the project and wrote the manuscript.

Data Availability Statement

Research data are not shared.

Keywords

cancer, carbon nanotubes, CDK1 kinase, fluorescence, peptide biosensors

Received: November 14, 2020
Revised: December 25, 2020
Published online: January 27, 2021

[1] D. Fabbro, S. W. Cowan-Jacob, H. Moebitz, *Br. J. Pharmacol.* **2015**, *172*, 2675.
[2] E. D. Fleuren, L. Zhang, J. Wu, R. J. Daly, *Nat. Rev. Cancer* **2016**, *16*, 83.
[3] S. Lim, P. Kaldis, *Development* **2013**, *140*, 3079.
[4] M. Malumbres, M. Barbacid, *Trends Biochem. Sci.* **2005**, *30*, 630.
[5] M. Malumbres, M. Barbacid, *Nat. Rev. Cancer* **2001**, *1*, 222.
[6] M. Malumbres, M. Barbacid, *Curr. Opin. Genet. Dev.* **2007**, *17*, 60.
[7] M. Malumbres, M. Barbacid, *Nat. Rev. Cancer* **2009**, *9*, 153.
[8] S. Lapenna, A. Giordano, *Nat. Rev. Drug Discovery* **2009**, *8*, 547.
[9] U. Asghar, A. K. Witkiewicz, N. C. Turner, E. S. Knudsen, *Nat. Rev. Drug Discovery* **2015**, *14*, 130.
[10] D. Santamaría, C. Barrière, A. Cerqueira, S. Hunt, C. Tardy, K. Newton, J. F. Cáceres, P. Dubus, M. Malumbres, M. Barbacid, *Nature* **2007**, *448*, 811.
[11] D. O. Morgan, *Annu. Rev. Cell Dev. Biol.* **1997**, *13*, 261.
[12] T. N. N. Van, M. C. Morris, *Prog. Mol. Biol. Transl. Sci.* **2013**, *113*, 217.
[13] M. C. Morris, *ACS Chem. Med. Lett.* **2014**, *5*, 99.
[14] A. E. Palmer, Y. Qin, J. G. Park, J. E. McCombs, *Trends Biotechnol.* **2011**, *29*, 144.
[15] J. A. González-Vera, M. C. Morris, *Proteomes* **2015**, *3*, 369.
[16] T. N. N. Van, S. Lykaso, M. Pellerano, M. C. Morris, *ChemBioChem* **2014**, *15*, 2298.
[17] C. Prével, C. M. Pellerano, J. A. González-Vera, P. Henri, L. Meunier, J. Vollaire, V. Josserand, M. C. Morris, *Biosens. Bioelectron.* **2016**, *85*, 371.
[18] M. Peyressatre, A. Laure, M. Pellerano, H. Boukhaddaoui, I. Soussi, M. C. Morris, *Biotechnol. J.* **2020**, *15*, 1900474.
[19] C. J. Serpell, K. Kostarelos, B. G. Davis, *ACS Cent. Sci.* **2016**, *2*, 190.
[20] N. Panwar, A. M. Soehartono, K. K. Chan, S. Zeng, G. Xu, J. Qu, P. Coquet, K.-T. Yong, X. Chen, *Chem. Rev.* **2019**, *119*, 9559.
[21] K. P. Loh, D. Ho, G. N. C. Chiu, D. T. Leong, G. Pastorin, E. K.-H. Chow, *Adv. Mater.* **2018**, *30*, 1802368.
[22] D. Chen, C. A. Dougherty, K. Zhu, H. Hong, *J. Controlled Release* **2015**, *210*, 230.
[23] B.-P. Jiang, B. Zhou, Z. Lin, H. Liang, X.-C. Shen, *Chem. - Eur. J.* **2019**, *25*, 3993.
[24] C.-M. Tîlmaciu, M. C. Morris, *Front. Chem.* **2015**, *3*, 59.
[25] S. Kumar, R. Rani, N. Dilbaghi, K. Tankeshwar, K.-H. Kim, *Chem. Soc. Rev.* **2017**, *46*, 158.
[26] B. Pei, W. Wang, N. Dunne, X. Li, *Nanomaterials* **2019**, *9*, 1501.
[27] G. Lamanna, A. Battigelli, C. Ménard-Moyon, A. Bianco, *Nanotechnol. Rev.* **2012**, *1*, 17.
[28] L. Chio, J. T. Del Bonis-O'Donnell, M. A. Kline, J. H. Kim, I. R. McFarlane, R. N. Zuckermann, M. P. Landry, *Nano Lett.* **2019**, *19*, 7563.
[29] J. T. Wang, R. Klippstein, M. Martincic, E. Pach, R. Feldman, M. Šefl, Y. Michel, D. Asker, J. K. Sosabowski, M. Kalbac, T. Da Ros, C. Ménard-Moyon, A. Bianco, I. Kyriakou, D. Emfietzoglou, J.-C. Saccavini, B. Ballesteros, K. T. Al-Jamal, G. Tobias, *ACS Nano* **2020**, *14*, 129.
[30] H. Kafa, J. T.-W. Wang, N. Rubio, R. Klippstein, P. M. Costa, H. A. F. M. Hassan, J. K. Sosabowski, S. S. Bansal, J. E. Preston, N. J. Abbott, K. T. Al-Jamal, *J. Controlled Release* **2016**, *225*, 217.
[31] K. T. Al-Jamal, H. Nerl, K. H. Müller, H. Ali-Boucetta, S. Li, P. D. Haynes, J. R. Jinschek, M. Prato, A. Bianco, K. Kostarelos, A. E. Porter, *Nanoscale* **2011**, *3*, 2627.
[32] B. Dinesh, A. Bianco, C. Ménard-Moyon, *Nanoscale* **2016**, *8*, 18596.
[33] H. Ali-Boucetta, A. Nunes, R. Sainz, M. A. Herrero, B. Tian, M. Prato, A. Bianco, K. Kostarelos, *Angew. Chem., Int. Ed.* **2013**, *52*, 2274.
[34] D. A. Heller, P. V. Jena, M. Pasquali, K. Kostarelos, L. G. Delogu, R. E. Meidl, S. V. Rotkin, D. A. Scheinberg, R. E. Schwartz, M. Terrones, Y. H. Wang, A. Bianco, A. A. Boghossian, S. Cambré, L. Cognet, S. R. Corrie, P. Demokritou, S. Giordani, T. Hertel, T. Ignatova, M. F. Islam, N. M. Iverson, A. Jagota, D. Janas, J. Kono, S. Kruss, M. P. Landry, Y. Li, R. Martel, S. Maruyama, et al, *Nat. Nanotechnol.* **2020**, *15*, 164.
[35] O. Gavet, J. Pines, *Dev. Cell* **2010**, *18*, 533.
[36] J. V. Frangioni, *Curr. Opin. Chem. Biol.* **2003**, *7*, 626.
[37] L. Kurzawa, M. Pellerano, J. B. Coppolani, M. C. Morris, *PLoS One* **2011**, *6*, e2655.
[38] I. Marangon, C. Ménard-Moyon, J. Kolosnjaj-Tabi, M. L. Béoutis, L. Lartigue, D. Alloyeau, E. Pach, B. Ballesteros, G. Autret, T. Ninjbadgar, D. F. Brougham, A. Bianco, F. Gazeau, *Adv. Funct. Mater.* **2014**, *24*, 7173.
[39] R. Singh, D. Pantarotto, L. Lacerda, G. Pastorin, C. Klumpp, M. Prato, A. Bianco, K. Kostarelos, *Proc. Natl. Acad. Sci. USA* **2006**, *103*, 3357.
[40] L. T. Vassilev, *Cell Cycle* **2006**, *5*, 2555.

